

MODAL ESTIMATION ON A WARPED FREQUENCY AXIS FOR LINEAR SYSTEM MODELING

A PREPRINT

 **Orchisama Das***
Institute of Sound Recording,
University of Surrey
Guildford, GU2 7XH, UK
o.das@surrey.ac.uk

Jonathan S. Abel
Center for Computer Research in Music and Acoustics
Stanford University
Stanford, CA 94305, USA
abel@ccrma.stanford.edu

ABSTRACT

Linear systems such as room acoustics and string oscillations may be modeled as the sum of mode responses, each characterized by a frequency, damping and amplitude. Here, we consider finding the mode parameters from impulse response measurements, and estimate the mode frequencies and decay rates as the generalized eigenvalues of Hankel matrices of system response samples, similar to ESPRIT. For greater resolution at low frequencies, such as desired in room acoustics and musical instrument modeling, the estimation is done on a warped frequency axis. The approach has the benefit of selecting the number of modes to achieve a desired fidelity to the measured impulse response. An optimization to further refine the frequency and damping parameters is presented. The method is used to model coupled piano strings and room impulse responses, with its performance comparing favorably to FZ-ARMA.

Keywords System Identification · Frequency Warping · ESPRIT

1 Introduction

Modal structures are an efficient way to synthesize acoustic spaces and vibrating systems. Modes originate from standing waves — they are exponentially damped sinusoids that are characterized by their frequencies, amplitudes and decay rates. These damped sinusoids are eigenfunctions of the acoustic transfer function between the input and output pressure waves. Modal analysis aims to estimate these parameters, and modal synthesis resynthesizes the analyzed sound using a bank of parallel biquad filters, each implementing one mode [1].

In [2], mode frequencies of a room are estimated by finding peaks in the power spectrum of the impulse response, and decay rates are approximated using reverberation times in bands about the estimated mode frequencies. Since rooms have thousands of modes, it is common-practice to estimate them on a band-by-band basis [2, 3]. Mode frequencies of carillon bells are estimated similarly in [4], and the decay rates are found with non-linear optimization [5]. Frequency-zoomed ARMA modeling on filtered groups of resonant frequencies has been used to model noisy string instruments and room responses in [6]. In [7, 8], modal parameters are estimated on a subband basis from the generalized eigenvalues of shifted Hankel matrices formed with impulse response samples. The method in [8] is computationally identical to ESPRIT [9], and was first formalized by Hua and Sarkar in [10]. In [8], the number of modes in each band is determined by k-means clustering, whereas in [7], they are determined by the relative magnitude of the singular values of the Hankel matrix. Modal parameter estimation with ESPRIT for modeling impulse responses has also recently been explored in [11].

Frequency warping [12] replaces the unit digital delay operator with a first order allpass filter with a non-uniform group delay. A cascade of allpass sections introduces non-uniform group delay, where the low-frequency components are delayed in time and the high frequency components get advanced. A warped frequency axis emphasizes psychoa-

*Use footnote for providing further information about author (webpage, alternative address)—*not* for acknowledging funding agencies.

coustic perception with more resolution in low frequencies. Warped digital filters have applications in loudspeaker equalization, linear predictive coding and physical modeling. Warping an impulse response has the effect of spreading out low-frequency modes around the unit circle, so that beating frequencies can be separated and resolved. Resolution of closely spaced sinusoids is important in modeling coupled vibrations. Some methods to address this problem include subspace methods such as [13], or spectral windowing methods such as the one used in [4]. However these methods require parameter tuning or are computationally expensive. In this paper, we perform modal estimation on a warped impulse response to resolve low-frequency beating modes.

Once the mode frequencies and dampings are estimated from the warped signal, we unwarped and optimize them. A sequential time-domain optimization scheme inspired by [14] is used. The mode amplitudes are re-estimated using least squares in each iteration. This kind of sequential optimization with consecutive update of the linear and non-linear parameters has also been used in [15]. This is different from [3, 16] where Maestre et al. fine-tune initial estimates of mode parameters with frequency-domain pole optimization.

This paper is organized as follows. We first discuss modal parameter estimation with ESPRIT in Section 2 and frequency-zoomed modal estimation with subband ESPRIT in Section 3. We introduce the frequency warped modal estimator in Section 4.1, and propose a new time-domain mode optimization method in Section 4.2. In Section 5, we discuss two applications of the proposed method — modal estimation of coupled piano strings (Section 5.1) and room impulse responses (Section 5.2). Each piano key (except the lower keys) is associated with sets of two or three strings coupled at the bridge. These strings are tuned with a small frequency deviation. String coupling leads to two-stage decay and beating [17, 18]. Room impulse responses also have a dense distribution of closely-spaced modes, some of which decay rapidly. Finally, we discuss the advantages of our method in Section 6 and conclude the paper in Section 7.

2 Modal Estimation

When a string is struck or plucked or a room is excited, traveling waves move in opposite directions, get reflected at the bridge or walls, and keep traveling back and forth. The resultant motion creates standing waves. The standing waves dissipate energy with time because of scattering and absorption. These standing waves, or modes of vibration, are damped sinusoids vibrating at natural frequencies of the system. Diagonalizing the second order partial differential equation of the one-dimensional traveling wave on a string, or three-dimensional traveling wave in a room yields damped sinusoids as the eigenfunctions of the system. The resulting vibration is due to the combination of several modes.

A discrete-time modeled signal $\hat{h}(t), t = 0, 1, \dots, T$, represented by a rational system without repeated poles, can be written as a sum of M modes,

$$\hat{h}(t) = \sum_{m=1}^M \gamma_m e^{(j\omega_m - \alpha_m)t} \quad (1)$$

where ω_m is the angular frequency, α_m is the decay rate and γ_m is the complex amplitude of the m th mode. The goal is to estimate the mode parameters from a noisy measurement of the signal, $h(t)$. The modal reconstruction filter is formed with a parallel bank of M second order filters, each synthesizing one mode. The Z-domain representation of the modeled signal $\hat{H}(z)$ is a sum of biquad filter transfer functions, i.e.,

$$\begin{aligned} \hat{H}(z) &= \mathcal{Z} \left(\sum_{m=1}^M \Re(h_m(t)) \right) \\ &= \sum_{m=1}^M \frac{\Re(\gamma_m) - e^{-\alpha_m} \Re(\gamma_m e^{-j\omega_m}) z^{-1}}{1 - 2e^{-\alpha_m} \cos \omega_m z^{-1} + e^{-2\alpha_m} z^{-2}} \end{aligned} \quad (2)$$

where \Re denotes the real part of a complex number.

Consider a Vandermonde matrix, \mathbf{V} , with the m th column, \mathbf{v}_m , representing the time series of the m th mode, $h_m(t)$

$$\begin{aligned} \mathbf{V} &= [\mathbf{v}_1 \quad \mathbf{v}_2 \quad \dots \quad \mathbf{v}_M] \\ \mathbf{v}_m &= [e^{-(j\omega_m - \alpha_m)0} \quad \dots \quad e^{-(j\omega_m - \alpha_m)\frac{T}{2}}]^\text{H} \end{aligned} \quad (3)$$

where H denotes Hermitian transpose. The Hankel matrix formed by the signal samples, \mathbf{H} , can be written as an outer product of the Vandermonde matrix \mathbf{V} with a diagonal matrix of mode amplitudes, $\mathbf{\Gamma} = \text{diag}[\gamma_1, \dots, \gamma_M]$.

$$\mathbf{H} = \begin{bmatrix} h(0) & h(1) & \dots & h(\frac{T}{2}) \\ h(1) & h(2) & \dots & h(\frac{T}{2} + 1) \\ \vdots & \vdots & \ddots & \vdots \\ h(\frac{T}{2}) & h(\frac{T}{2} + 1) & \dots & h(T) \end{bmatrix} \quad (4)$$

$$\mathbf{H} = \mathbf{V}\mathbf{T}\mathbf{V}^H \quad (5)$$

Similar to ESPRIT [9], the Hankel matrix offset by 1 sample, \mathbf{K} , can be written as

$$\mathbf{K} = \begin{bmatrix} h(1) & h(2) & \dots & h(\frac{T}{2} + 1) \\ h(2) & h(3) & \dots & h(\frac{T}{2} + 2) \\ \vdots & \vdots & \ddots & \vdots \\ h(\frac{T}{2} + 1) & h(\frac{T}{2} + 2) & \dots & h(T + 1) \end{bmatrix} \quad (6)$$

$$\mathbf{K} = \mathbf{V}\mathbf{\Psi}\mathbf{T}\mathbf{V}^H \quad (7)$$

where $\mathbf{\Psi} = \text{diag} [e^{(j\omega_1 - \alpha_1)} \dots e^{(j\omega_M - \alpha_M)}]$. Post multiplying \mathbf{K} with the pseudoinverse of \mathbf{H} , we get

$$\mathbf{K}\mathbf{H}^\dagger = \mathbf{V}\mathbf{\Psi}\mathbf{V}^{-1} \quad (8)$$

Thus, the diagonal elements of $\mathbf{\Psi}$ are the generalized eigenvalues of the matrix pencil (\mathbf{K}, \mathbf{H}) . The mode frequency and damping estimates are the imaginary and real parts of the logarithm of the eigenvalues, ψ_m ,

$$\ln \psi_m = j\omega_m - \alpha_m \quad (9)$$

The number of modes, M , is estimated by the rank of the matrix \mathbf{H} (by its largest singular values). The mode amplitudes, γ , are found by least squares fit to the measured signal.

$$\gamma = \mathbf{V}^\dagger \mathbf{h} \quad (10)$$

where \mathbf{V}^\dagger is the pseudoinverse of the Vandermonde matrix formed from the mode frequencies and dampings.

3 Frequency-zoomed Modeling

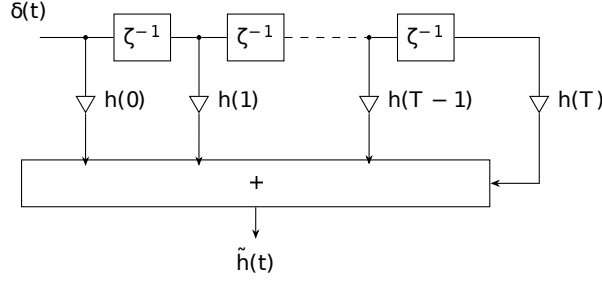
The modal estimation method described in Section 2 can be done on a frequency band-by-band basis. The signal, $h(t)$, is filtered into overlapping frequency bands, and downsampled. This process ensures that each band has relatively few modes to be estimated that are well separated in frequency. In other words, subband processing puts a magnifying glass on the frequency spectrum, and helps resolve close frequency beating modes. Furthermore, downsampling effectively increases the pole damping.

Let us consider N_b bands at a sampling rate of f_s Hz, each with band center at f_n Hz, $f_n = (2n - 1)f_s/4N_b$, $n = 1, 2, \dots, N_b$. The impulse response is heterodyned by multiplying with a complex exponential tuned to the band centers,

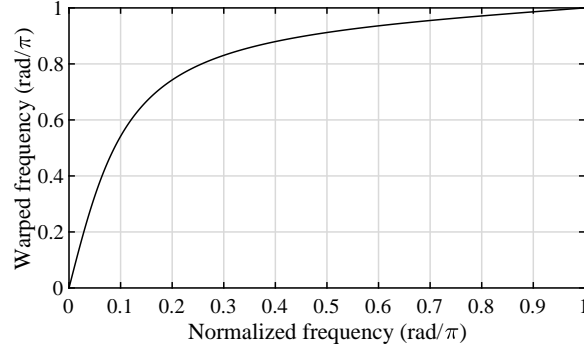
$$h_n(t) = h(t) \exp(-2\pi j f_n t). \quad (11)$$

The heterodyned signal, $h_n(t)$, which is now centered at DC, is then filtered with a high-order LPF with a narrow passband. The filtered signal is decimated by a factor of r . The mode frequencies and dampings are estimated for each band as $\hat{f}_{m,n}$ and $\hat{\alpha}_{m,n}$. Mode frequencies are moved up the spectrum to $\hat{f}_{m,n} + f_n$ to undo the effect of heterodyne, and mode amplitudes are adjusted as $\sqrt[r]{\hat{\alpha}_{m,n}}$ to undo the effect of downsampling. Modes from subsequent bands are concatenated after discarding modes in overlapping passbands.

This process is comparable to FZ-ARMA [6] where the signal is also processed in frequency bands, heterodyned and downsampled before detecting ARMA model coefficients with Steiglitz-McBride iteration. Therefore, we will refer to this method as FZ-ESPRIT (Frequency-Zoomed ESPRIT) henceforth in this paper. One advantage of modeling the system as second order filters in parallel versus a large order polynomial, as is the case in ARMA models, is that numerical methods such as Steiglitz McBride can be unstable with high order models, whereas ESPRIT is numerically robust and gives stable solutions. Moreover, model order selection in FZ-ARMA is not straightforward, whereas in FZ-ESPRIT, the number of modes in any frequency band are picked based on the magnitude of the singular values of the Hankel matrix.



(a) Warping an impulse response



(b) Frequency warping as conformal mapping

Figure 1: Frequency warping with allpass sections.

4 Proposed Method

4.1 Frequency warped modal estimation

As an alternative to the subband processing that is done in FZ-ARMA and FZ-ESPRIT, we propose Frequency-Warped ESPRIT (FW-ESPRIT). FW-ESPRIT warps the second order modal filters such that their poles become more damped and further apart in frequency. Frequency warping [12] warps a uniform frequency axis to a non-uniform one. Warping is done by replacing the unit delay z^{-1} with a first-order allpass filter ζ^{-1} , given by:

$$\zeta^{-1} = \frac{z^{-1} - \rho}{1 - \rho z^{-1}} \quad (12)$$

where ρ is the warping factor. Figure 1b shows the mapping between natural frequencies, ω , and warped frequencies, $\tilde{\omega}$, determined by the phase of the allpass filter in Eq. (12). The negative group delay of this allpass filter gives the slope of the mapping as a function of frequency,

$$\tilde{\omega} = \arctan \left(\frac{(1 - \rho^2) \sin \omega}{(1 + \rho^2) \cos \omega - 2\rho} \right) \quad (13)$$

$$\frac{d\tilde{\omega}}{d\omega} = -\frac{1 - \rho^2}{1 + \rho^2 - 2\rho \cos \omega}.$$

By choosing an appropriate warping factor, ρ^* , we can map uniformly spaced points on the frequency axis to a non-uniformly spaced warped frequency axis, such as approximating a Bark scale, as shown in Fig. 1b. For a sampling frequency of f_s Hz, the optimal warping factor for Bark mapping is given by

$$\rho^* = 1.0674 \left[\frac{2}{\pi} \arctan(0.6583 f_s) \right]^{0.5} - 0.1916 \quad (14)$$

which approximately equals 0.75 for $f_s = 44.1$ kHz, [19].

For modes near DC, warping increases the frequency by a factor of $(1 + \rho)/(1 - \rho)$. High-frequency modes near the band-edge get compressed by a factor of $(1 - \rho)/(1 + \rho)$. Similarly, the decay times of the low-frequency modes

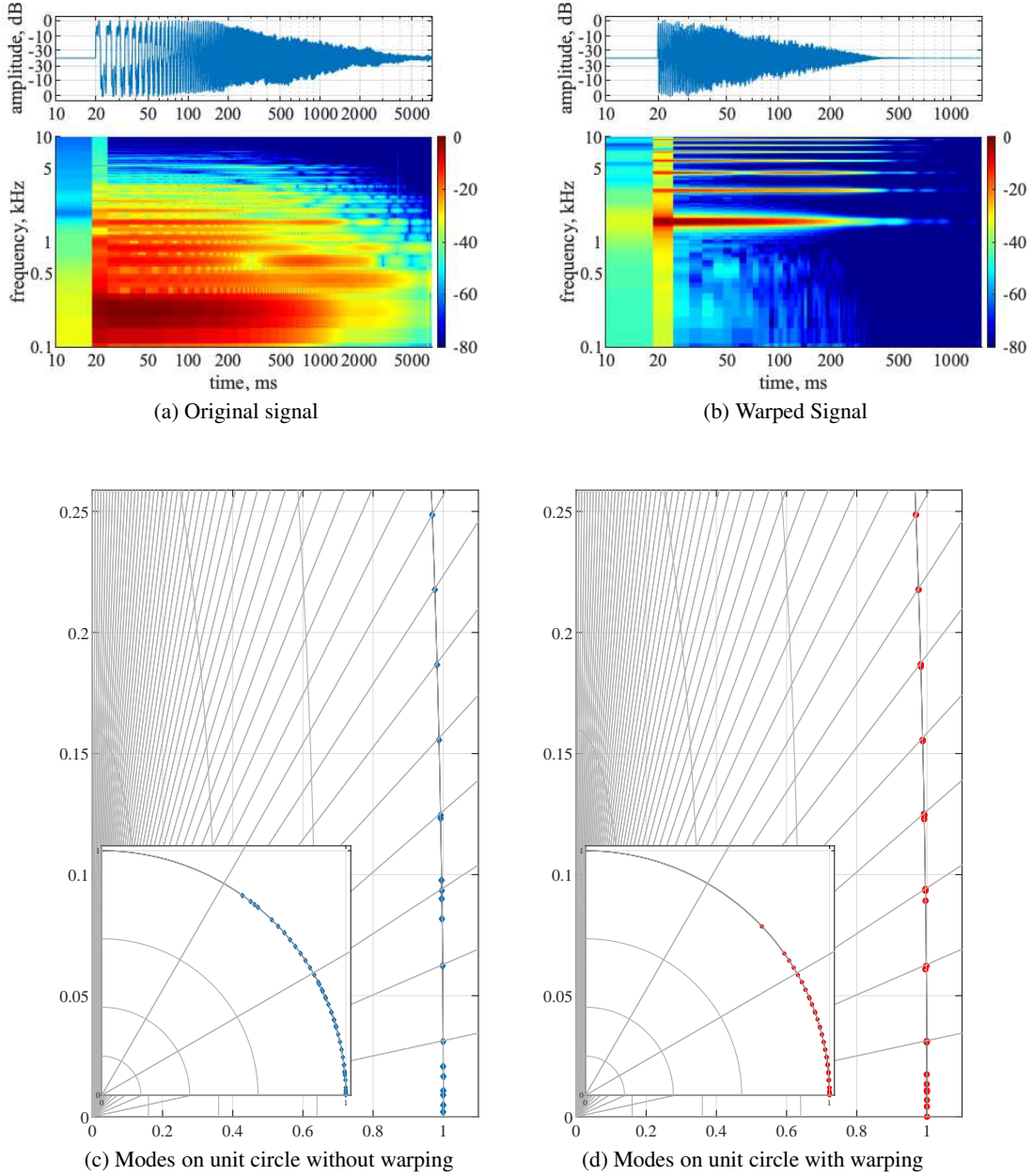


Figure 2: Top - Original and warped signal waveform and spectrogram on a log time axis. Bottom - Estimated modes with warping (red circles) and without warping (blue diamonds). Left - modes in z-plane with direct estimation. Right - modes in z-plane after unwarping. The plots are zoomed in up to a polar angle of $\frac{\pi}{12}$ rad (1837.5 Hz) to show the lower frequency modes, and grey lines are at harmonics of the fundamental.

are decreased by a factor of $(1 + \rho)/(1 - \rho)$, and that of the high-frequency modes are increased by a factor of $(1 - \rho)/(1 + \rho)$. The choice of the warping factor should depend on the application, and how much frequency zooming is desired. For a zooming factor of K_z in the lower frequencies, the warping factor can be selected as $\rho = \frac{K_z - 1}{K_z + 1}$.

To warp a signal or an impulse response, $h(t)$, the filter structure in Fig. 1a needs to be implemented. As a result of the warping, the signal frequencies have non-uniform group delay. The original and warped piano signals with $\rho = \rho^*$ are shown in Fig. 2a, 2b. As visible in the frequency domain, the modes in the warped response have been shifted to higher and further spaced frequencies, and their dampings have been increased (approximately by a factor of 7).

To estimate the modes, we first warp the response, estimate the warped modal parameters, and unwarp the frequencies and dampings before estimating the amplitudes using the unwrapped impulse response. The measured signal is warped with a warping factor of ρ^* (Eq. 14) and its modes are estimated using the method described in Section 2.

Modal estimation with frequency warping overlooks some high frequency modes because of compression of the frequency axis near the band-edge. These modes are required for accurate reconstruction of the transient. As a workaround, two sets of modes are calculated from the signal, one with and one without frequency warping. A combined set of modes is used, with lower frequency modes from the warped set and higher frequency modes from the non-warped set. A frequency cutoff threshold, ω_c , is selected for combining the modes by setting the slope of the mapping to 1, where the warped frequency is equal to the non-warped frequency. This gives $\omega_c = \cos^{-1}(\rho)$. To unwarp the mode frequencies and dampings, the poles are unwrapped, and Eq. (9) is used to get the mode frequencies and dampings from the unwrapped poles.

$$\begin{aligned}\tilde{\psi}_m &= e^{(j\tilde{\omega}_m - \tilde{\alpha}_m)} \\ \psi_m &= \frac{-\rho + \tilde{\psi}_m^*}{1 - \rho\tilde{\psi}_m^*}.\end{aligned}\tag{15}$$

The modes estimated from the three coupled strings of a measured piano note at 220 Hz, without and with frequency warping are plotted as poles on the z-plane in Figs. 2c, 2d respectively. Beating modes can be clearly seen in Fig. 2d, where overlapping circles in the zoomed plot indicate triplets caused by the three coupled strings vibrating together. Low-frequency beating modes are captured by frequency warping, which are otherwise missed in the non-warped case.

4.2 Mode optimization

To fine-tune the estimated modes, we propose a new time-domain iterative mode optimization method. The modeled signal, $\hat{h}(t)$, Eq. (1) can also be written as

$$\hat{h}(t) = \sum_{m=1}^M e^{-\alpha_m t} [\gamma_{s_m} \sin(\omega_m t) + \gamma_{c_m} \cos(\omega_m t)]\tag{16}$$

where $\gamma_{s_m}, \gamma_{c_m}$ are the real mode amplitudes associated with the sine and cosine components of the m th mode. Using Eq. (16) has the advantage of making the cost function real. In vector form, Eq. (16) can be written as

$$\begin{aligned}\hat{\mathbf{h}} &= [\Im(\mathbf{V}) \quad \Re(\mathbf{V})] \begin{bmatrix} \gamma_s \\ \gamma_c \end{bmatrix} \\ &= \begin{bmatrix} e^{-\alpha_1 0} \sin(\omega_1 0) & \cdots & e^{-\alpha_M 0} \cos(\omega_M 0) \\ \vdots & \cdots & \vdots \\ \vdots & \cdots & \vdots \\ \vdots & \cdots & \vdots \\ e^{-\alpha_1 T} \sin(\omega_1 T) & \cdots & e^{-\alpha_M T} \cos(\omega_M T) \end{bmatrix} \begin{bmatrix} \gamma_{s1} \\ \vdots \\ \gamma_{sM} \\ \gamma_{c1} \\ \vdots \\ \gamma_{cM} \end{bmatrix}\end{aligned}\tag{17}$$

We can now form a vector of mode dampings and frequencies, $\theta = [\alpha^T \ \omega^T]$ to optimize. The time-domain non-linear cost function and its gradient are

$$\begin{aligned}J(\theta) &= \frac{1}{2} \|\mathbf{h} - \hat{\mathbf{h}}(\theta)\|_2^2 \\ &= \frac{1}{2} (\mathbf{h} - \hat{\mathbf{h}}(\theta))^\top (\mathbf{h} - \hat{\mathbf{h}}(\theta)) \\ \nabla_\theta J(\theta) &= D_\theta(\hat{\mathbf{h}}(\theta))^\top [\hat{\mathbf{h}}(\theta) - \mathbf{h}]\end{aligned}\tag{18}$$

where \mathbf{h} is the measured signal vector, $\hat{\mathbf{h}}(\theta)$ is the modeled signal vector and $D_\theta(\hat{\mathbf{h}}(\theta)) \in \mathbb{R}^{T \times 2M}$ is the Jacobian matrix of $\hat{\mathbf{h}}(\theta)$ with respect to θ . Each entry of the Jacobian matrix is given by

$$\begin{aligned} D_\theta(t, m) &= \frac{\partial \hat{\mathbf{h}}(t)}{\partial \alpha_m} \\ &= -te^{-\alpha_m t} [\gamma_{s_m} \sin(\omega_m t) + \gamma_{c_m} \cos(\omega_m t)] \\ D_\theta(t, 2m) &= \frac{\partial \hat{\mathbf{h}}(t)}{\partial \omega_m} \\ &= te^{-\alpha_m t} [\gamma_{s_m} \cos(\omega_m t) - \gamma_{c_m} \sin(\omega_m t)] \end{aligned} \quad (19)$$

For faster computation, we bandpass filter the signal into several frequency bands and optimize the modes in each band. We use MATLAB's `fmincon` optimizer with initial mode parameter estimates calculated from Section 2. The amplitudes $\gamma_{s_m}, \gamma_{c_m}$ are re-calculated in each iteration of the optimization using least squares.

Providing `fmincon` with the gradient of the cost function speeds up computation significantly. We also set constraints such that $\omega_{0_m} - \delta_\omega < \omega_m < \omega_{0_m} + \delta_\omega$ and $\alpha_{0_m} - \delta_\alpha < \alpha_m < \alpha_{0_m} + \delta_\alpha$, where ω_0 and α_0 are the initial estimates and $\delta_\omega, \delta_\alpha$ are the maximum deviations allowed from the initial point. We ensure the mode frequencies are ordered in ascending order, i.e., $\omega_{m-1} \leq \omega_m \leq \omega_{m+1}$.

The cost function is non-convex, so converging to a local minimum is probable. To avoid this, the initial estimate has to be close to the global optimum. We run the optimizer for a maximum of 500 function counts and convergence is achieved if the error is small enough ($\leq 1e-4$), or the step size calculated by `fmincon` is small enough ($\leq 1e-9$).

Algorithm 1 Mode optimization pseudocode

Require: $\alpha_{b,0} - \delta_\alpha \leq \theta_{1:M} \leq \alpha_{b,0} + \delta_\alpha, \omega_{0,b} - \delta_\omega \leq \theta_{M+1:2M} \leq \omega_{b,0} + \delta_\omega \forall b$
for $b = 1, \dots, N_b$ **do**
 $\theta_0 = [\alpha_{b,0} \ \omega_{b,0}]^\top$
 repeat
 $\hat{\mathbf{h}}(\theta_i) \leftarrow [\Im(\mathbf{V}(\theta_i)) \ \Re(\mathbf{V}(\theta_i))] \begin{bmatrix} \gamma_s \\ \gamma_c \end{bmatrix}$
 $J(\theta_i) \leftarrow 0.5 \|\mathbf{h} - \hat{\mathbf{h}}(\theta_i)\|^2$
 $\theta_{i+1} \leftarrow \arg \min_\theta J(\theta_i)$
 $[\gamma_s \ \gamma_c]^\top \leftarrow [\Im(\mathbf{V}(\theta_{i+1})) \ \Re(\mathbf{V}(\theta_{i+1}))]^\dagger \mathbf{h}$
 until convergence
 $\alpha_b^*, \omega_b^* = \theta_i^*$
end for

5 Applications

5.1 Coupled Piano Strings

Coupled string systems typically have two or more strings coupled at a non-rigid bridge. The eigenanalysis of two strings coupled at a bridge is explained in [20]. The piano hammer striking the strings produces motion primarily in the transverse direction, but also in the longitudinal direction. The transverse vibrations are much stronger initially, but attenuate quickly whereas the weaker longitudinal vibrations persist. There is significant coupling between transverse and longitudinal vibrations [21]. Transverse vibrations produce modes at harmonic frequencies. The longitudinal motion is continuously excited by the transverse vibration along the string. The forced response to this excitation gives rise to phantom partials, while the free response produces the components corresponding to the longitudinal modal frequencies. The *aftersound*, or the second stage of a two-stage decay is caused by a combined effect of string coupling and shift from transverse to longitudinal polarization.

Coupled piano strings are slightly mistuned, and the amount of mistuning either causes audible beating (amplitude modulation), or a beatless *aftersound*. Coupled strings vibrate in phase immediately after impact, producing the *prompt* sound. Because their frequencies are slightly different, they become out of phase eventually. Once this phase offset becomes approximately a half period of one of the frequencies, the movement at the bridge almost completely cancels, and sound is sustained. Modal parameters of coupled strings can be used in conjunction with other physical models, such as digital waveguides, for more realistic sound synthesis. A hybrid modal-waveguide model has been used to synthesize coupled strings in [22]. Coupled digital waveguides have been used in [23].

Table 1: Mode estimation results without optimization

| Note | FW-ESPRIT | | | FZ-ESPRIT $r = 5000$ | | | FZ-ARMA $r = 5000$ | | |
|------|-----------|----------|------|----------------------|----------|-----|--------------------|----------|-----|
| | MSE (dB) | Time (s) | M | MSE (dB) | Time (s) | M | MSE (dB) | Time (s) | M |
| C1 | -118.25 | 13.43 | 61 | -101.07 | 21.16 | 290 | -101.11 | 35.87 | 666 |
| C2 | -94.97 | 27.52 | 119 | -94.16 | 28.13 | 528 | -94.35 | 37.51 | 720 |
| C3 | -106.95 | 25.61 | 349 | -91.49 | 42.56 | 628 | -91.63 | 38.17 | 720 |
| C4 | -113.47 | 83.24 | 1005 | -102.98 | 49.65 | 769 | -102.91 | 32.33 | 720 |

Table 2: Mode estimation results with optimization

| Note | FW-ESPRIT opt | | | FZ-ESPRIT opt $r = 5000$ | | | FZ-ARMA opt $r = 5000$ | | |
|------|---------------|----------|------|--------------------------|----------|------|------------------------|----------|------|
| | MSE (dB) | Time (s) | Iter | MSE (dB) | Time (s) | Iter | MSE (dB) | Time (s) | Iter |
| C1 | -119.52 | 20.34 | 93 | -110.52 | 13.85 | 1 | -110.71 | 14.63 | 1 |
| C2 | -95.04 | 69.14 | 424 | -93.59 | 30.83 | 154 | -95.51 | 57.38 | 214 |
| C3 | -108.66 | 96.13 | 305 | -95.79 | 26.81 | 142 | -99.91 | 48.57 | 125 |
| C4 | -111.44 | 48.22 | 118 | -116.77 | 23.99 | 74 | -112.04 | 41.72 | 136 |

We evaluated FW-ESPRIT against FZ-ESPRIT and FZ-ARMA on the MIS² dataset of piano recordings for the C note spanning four octaves, from 32.7 Hz (C1) to 261.6 Hz (C4)³. For FZ-ESPRIT, we warp the measured signal with a warping coefficient $\rho^* = -0.77$ (Eq. 14) at a sampling rate of $f_s = 44.1$ kHz. The order of the Hankel matrix used is $\mathbb{R}^{T \times T}$, $T = 2048$. A large order gives more accurate mode estimates at the cost of computational complexity. To determine the number of modes, M , we order the singular values by magnitude and find its *knee-point* [24].

For FZ-ESPRIT and FZ-ARMA, we center the bandpass filters around frequency f_n Hz after taking into account string stiffness [25] with an inharmonicity coefficient of $B = 10^{-4}$ and a fundamental frequency of f_0 Hz,

$$f_n = n f_0 \sqrt{1 + B n^2} \quad (20)$$

A fourth order Butterworth filter with a bandwidth of 1/10th the fundamental frequency is used. The downsampling factor is selected to be $K_z = 5000$. The ARMA model order is fixed to be 12, as suggested in [6]. For all methods, modes around the first 60 partials are estimated.

The time domain mean-squared errors without optimization are shown in Table 1. FW-ESPRIT outperforms the other two methods at a comparable run-time. For the ESPRIT based methods, computation time is directly proportional to the number of estimated modes. As the fundamental frequency increases, so does the number of modes. FZ-ARMA has mean-squared errors comparable to those of FZ-ESPRIT, since they essentially perform the same operations of downsampling, filtering and estimating. The ESPRIT based algorithms have an advantage over FZ-ARMA, since the detection of the number of modes is automatic.

The results of the proposed post-processing optimization scheme are shown in Table 2. Optimization parameters were selected to be $\delta_\alpha = 0.1\alpha_0$ and $\delta_\omega = 0.5$ Hz (window of 1 Hz around estimated mode frequencies). The third column of the table denotes the number of iterations to convergence. The total run-time of the optimization depends on this, as well as the number of modes being optimized. In general, optimization improves the mean-squared error, except in the case of C4 estimation with FW-ESPRIT. The computation time is reasonable for offline applications. The frequency spectrum of the measured and modeled signals with and without optimization are shown in Fig 3. Fits to the measured data is improved with optimization.

5.2 Room Impulse Response

The sound field in a room is given by the 3D wave equation [26],

$$\frac{\partial^2 p}{\partial t^2} = c^2 \left(\frac{\partial^2 p}{\partial x^2} + \frac{\partial^2 p}{\partial y^2} + \frac{\partial^2 p}{\partial z^2} \right) \quad (21)$$

where p is the acoustic pressure, c is the speed of sound in the medium, and x, y, z are Cartesian coordinates. The time-independent form of the wave equation in the Fourier domain is known as the Helmholtz equation, characterized

²<http://theremin.music.uiowa.edu/MISpiano.html>

³Sound examples are available at https://ccrma.stanford.edu/~orchi/Modal/warped_modal.html.

by the wave-number k ,

$$\frac{\partial^2 p}{\partial x^2} + \frac{\partial^2 p}{\partial y^2} + \frac{\partial^2 p}{\partial z^2} + k^2 p = 0 \quad (22)$$

The solutions to this equation are standing waves, or room modes. For a rectangular room with rigid walls and dimensions L_x, L_y and L_z in directions x, y, z respectively, the wave numbers, k , and mode frequencies, f , are given by

$$\begin{aligned} k^2 &= k_x^2 + k_y^2 + k_z^2; \quad f = \frac{c}{2\pi} k \\ k_\mu &= \frac{n_\mu \pi}{L_\mu}; \quad \mu \in (x, y, z), \quad n_\mu \in \mathbb{Z}^+ \end{aligned} \quad (23)$$

For varying values of n_x, n_y and n_z , a large number of axial, tangential and oblique modes are generated.

A room impulse response can be characterized by a sum over M such modes (1). The complex amplitudes, γ_m , are functions of space, determined by the source and receiver positions, whereas frequencies and dampings, ω_m and α_m , are properties of the room and its material. The idea of a modal reverberator is to implement the room modes using separate resonant filters, each driven by the source signal and summed in a parallel structure to form the output [2].

A medium sized classroom was measured and modeled with FW-ESPRIT, FZ-ESPRIT and FZ-ARMA. The Hankel matrix size for FW-ESPRIT was doubled to 4096 samples. The non-warped impulse response was multiplied with a damped exponential, $r^n = \exp(-1.5n/f_s)$, before applying ESPRIT to find its modes. This introduced some extra damping to the high frequency modes, i.e., it shrunk the pole radius. Once the modes were estimated, they were undamped by multiplying with $\frac{1}{r}$. After this, the two sets of modes from the warped and non-warped RIR were combined.

For one experiment, we selected the number of modes by finding the *knee-point* of the singular value curve of the Hankel matrix. This resulted in a good fit with $M = 2994$ modes, as shown in Fig. 4a. The decay rates of some high frequency modes are overestimated, but the optimization helps take care of that. For another experiment, the number of modes was chosen by finding the singular values whose magnitude was greater than -18 dB. This resulted in an SNR of -18 dB and $M = 1402$ modes. The results, shown in Fig. 4b, indicate a poorer fit with colored reverberation.

For FZ-ARMA and FZ-ESPRIT, the processing was done on a non-uniform filterbank approximating the Bark scale, with smaller bandwidth low frequency bands and longer bandwidth high frequency bands. There were $N_b = 20$ frequency bands for FZ-ESPRIT, and $N_b = 40$ bands for FZ-ARMA whose centers were uniformly distributed from $[0, \frac{f_s}{2}]$ Hz, with $f_s = 48$ kHz, and then warped according to Eq. (13). The filter bandwidth was selected as $\beta_b = 1.2 * ((f_{b+1} - f_b)/2)$ Hz. A 7th order Elliptic filter with a stop-band ripple of -80 dB, pass-band ripple of 1.5 dB and cutoff of β_b Hz was used. The results of FZ-ESPRIT are shown in Fig. 4c.

For FZ-ESPRIT, a maximum number of modes, $M_{b_{\max}} = 100$, was allotted per frequency band. If the mode budget was not exhausted in any band, the remaining mode budget was distributed equally among the other bands. This ensured that higher frequency bands with a greater bandwidth (which contain many rapidly decaying modes) had an adequate mode budget. The downsampling factor was $K_z = 8$.

For FZ-ARMA, the maximum allowed zero and pole order was set to $N_{\max} = 30$, $P_{\max} = 150$ respectively. The pole and zero order of each band was selected by a non-linear mapping of the bandwidth,

$$\begin{aligned} \beta_{bn} &= \frac{\beta_b}{\max_{b=1, \dots, N_b} \beta_b}, \quad \beta_{bn} \in (0, 1] \\ \{N, P\}_b &= \left\lfloor \frac{\tanh(3\beta_{bn})}{\tanh(3)} \times \{N, P\}_{\max} \right\rfloor \end{aligned} \quad (24)$$

where $\lfloor \cdot \rfloor$ denotes rounding operation to the nearest integer. This also ensures that the modes are distributed according to the filter bandwidths. The downsampling factor was selected to be $K_z = 100$. For all methods, the optimization window for the frequency estimates was set to $\delta_\omega = 2$ Hz, and a maximum of 100 iterations were run for each frequency band. The results are shown in Fig. 4d.

It is evident from the plots and the sound examples that FZ-ARMA fails at modeling the RIR. With the right selection of parameters, it can potentially model a certain narrow frequency range accurately, as discussed in [6]. Between FZ-ESPRIT and FW-ESPRIT, the former gives perceptually impressive results with almost half the number of modes.

6 Discussion

- Compared to FZ-ARMA, the ESPRIT based methods have the advantage of automatic order selection. The performance of ARMA modeling depends on the model orders selected, which needs to be done manually on a case-by-case basis. In the ESPRIT based methods, we algorithmically look at the magnitudes of the singular values of the Hankel matrix to make this decision.
- There are a few options for selecting the number of modes. One option is to look for the *knee-point* in the singular value curve, which indicates the point after which the curve drops off. This produces the best fit at the cost of picking a large number of modes. The other option is to choose an SNR for each frequency band, and pick the singular values whose magnitudes lie above the SNR. This method gives a constant SNR in each frequency band.
- FZ-ARMA needs a large downsampling factor to give reasonable results. A large downsampling factor can easily miss the fast decaying modes.
- In FZ-ESPRIT, one has to manually select the downsampling factor, number of frequency bands, transition frequencies and bandwidths. The only parameter that needs tuning in FW-ESPRIT is the warping coefficient.
- FZ-ARMA is inept at modeling RIR modes. FZ-ESPRIT produces the best perceptual results with fewer modes than FW-ESPRIT. FZ-ESPRIT is preferred for modeling RIRs, whereas FW-ESPRIT is ideal for modeling harmonic signals, such as those of musical instruments. All methods have been implemented in a modal estimation toolbox [27].

7 Conclusion

A modal estimation technique has been proposed, which operates on a warped frequency axis, and is well-suited to modeling low-frequency beating modes. Frequency warping gives higher resolution at low frequencies and increases damping of the modes. This method achieves results comparable to subband modal estimation (FZ-ESPRIT) with a computational advantage, and gets better fits than FZ-ARMA. To fine-tune the estimated mode parameters, the error between our model and the measured response has been optimized.

Two applications of the proposed method were demonstrated — modeling of coupled piano strings and room impulse responses. Subband filter design and model order selection was discussed in detail for all the methods. The results of FW-ESPRIT, compared with FZ-ESPRIT and FZ-ARMA, show the efficacy of the proposed method in modeling linear systems with densely distributed modes with minimal parameter tuning.

References

- [1] J.-M. Adrien, “The missing link: Modal synthesis,” in *Representations of musical signals*, 1991, pp. 269–298.
- [2] J. S. Abel, S. Coffin, and K. Spratt, “A modal architecture for artificial reverberation with application to room acoustics modeling,” in *Audio Engineering Society Convention 137*. Audio Engineering Society, 2014.
- [3] E. Maestre, J. S. Abel, J. O. Smith, and G. P. Scavone, “Constrained pole optimization for modal reverberation,” in *Proceedings of the International Conference on Digital Audio Effects (DAFx)*, 2017.
- [4] M. Rau, O. Das, and E. K. Canfield-Dafilou, “Improved carillon synthesis,” in *Proceedings of the International Conference on Digital Audio Effects (DAFx)*, 2019.
- [5] P. Antsalo, A. Makivirta, V. Valimäki, T. Peltonen, and M. Karjalainen, “Estimation of modal decay parameters from noisy response measurements,” in *Audio Engineering Society Convention 110*. Audio Engineering Society, 2001.
- [6] M. Karjalainen, P. A. Esquef, P. Antsalo, A. Mäkiavirta, and V. Välimäki, “Frequency-zooming ARMA modeling of resonant and reverberant systems,” *Journal of the Audio Engineering Society*, vol. 50, no. 12, pp. 1012–1029, 2002.
- [7] J. S. Abel, “Method and system for designing a modal filter,” September 3 2018, uS Patent App. No. 62-726325 (originally private communication, November 27 2017).
- [8] C. Kereliuk, W. Herman, R. Wedelich, and D. J. Gillespie, “Modal analysis of room impulse responses using subband ESPRIT,” in *Proceedings of the International Conference on Digital Audio Effects (DAFx)*, 2018.
- [9] R. Roy and T. Kailath, “ESPRIT-estimation of signal parameters via rotational invariance techniques,” *IEEE Transactions on acoustics, speech, and signal processing*, vol. 37, no. 7, pp. 984–995, 1989.

-
- [10] Y. Hua and T. K. Sarkar, "Matrix pencil method for estimating parameters of exponentially damped/undamped sinusoids in noise," *IEEE Transactions on Acoustics, Speech, and Signal Processing*, vol. 38, no. 5, pp. 814–824, 1990.
- [11] J. J. Wells, "Modal decompositions of impulse responses for parametric interaction," *Journal of the Audio Engineering Society*, vol. 69, no. 7/8, pp. 530–541, 2021.
- [12] A. Härmä, M. Karjalainen, L. Savioja, V. Välimäki, U. K. Laine, and J. Huopaniemi, "Frequency-warped signal processing for audio applications," *Journal of the audio engineering society*, vol. 48, no. 11, pp. 1011–1031, 2000.
- [13] O. Das, J. S. Abel, and J. O. Smith III, "FAST MUSIC—an efficient implementation of the MUSIC algorithm for frequency estimation of approximately periodic signals," in *Proceedings of the International Conference on Digital Audio Effects (DAFx)*, 2018.
- [14] P. Ainsleigh and J. George, "Modeling exponential signals in a dispersive multipath environment," in *Proceedings of ICASSP-92: 1992 IEEE International Conference on Acoustics, Speech, and Signal Processing*, vol. 5. IEEE, 1992, pp. 457–460.
- [15] O. Das, P. Calamia, and S. V. Amengual Gari, "Room impulse response interpolation from a sparse set of measurements using a modal architecture," in *IEEE International Conference on Acoustics, Speech and Signal Processing (ICASSP)*. IEEE, 2021, pp. 960–964.
- [16] E. Maestre, G. P. Scavone, and J. O. Smith, "Design of recursive digital filters in parallel form by linearly constrained pole optimization," *IEEE Signal Processing Letters*, vol. 23, no. 11, pp. 1547–1550, 2016.
- [17] G. Weinreich, "Coupled piano strings," *The Journal of the Acoustical Society of America*, vol. 62, no. 6, pp. 1474–1484, 1977.
- [18] ———, "The coupled motions of piano strings," *Scientific American*, vol. 240, no. 1, pp. 118–127, 1979.
- [19] J. O. Smith and J. S. Abel, "Bark and ERB bilinear transforms," *IEEE Transactions on speech and Audio Processing*, vol. 7, no. 6, pp. 697–708, 1999.
- [20] J. O. Smith, *Physical audio signal processing: For virtual musical instruments and audio effects*. W3K publishing, 2010.
- [21] B. Bank and L. Sujbert, "Generation of longitudinal vibrations in piano strings: From physics to sound synthesis," *The Journal of the Acoustical Society of America*, vol. 117, no. 4, pp. 2268–2278, 2005.
- [22] N. Lee, J. O. Smith, and V. Valimaki, "Analysis and synthesis of coupled vibrating strings using a hybrid modal-waveguide synthesis model," *IEEE transactions on audio, speech, and language processing*, vol. 18, no. 4, pp. 833–842, 2009.
- [23] M. Aramaki, J. Bensa, L. Daudet, P. Guillemain, and R. Kronland-Martinet, "Resynthesis of coupled piano string vibrations based on physical modeling," *Journal of New Music Research*, vol. 30, no. 3, pp. 213–226, 2001.
- [24] D. Kaplan, "Knee point Matlab Central File Exchange," 2021. [Online]. Available: <https://www.mathworks.com/matlabcentral/fileexchange/35094-knee-point>
- [25] R. W. Young, "Inharmonicity of plain wire piano strings," *The Journal of the Acoustical Society of America*, vol. 24, no. 3, pp. 267–273, 1952.
- [26] H. Kuttruff, *Room Acoustics*. CRC Press, 2016.
- [27] O. Das, "Modal estimation toolbox," 2021. [Online]. Available: <https://github.com/orchidas/Modal-estimation>

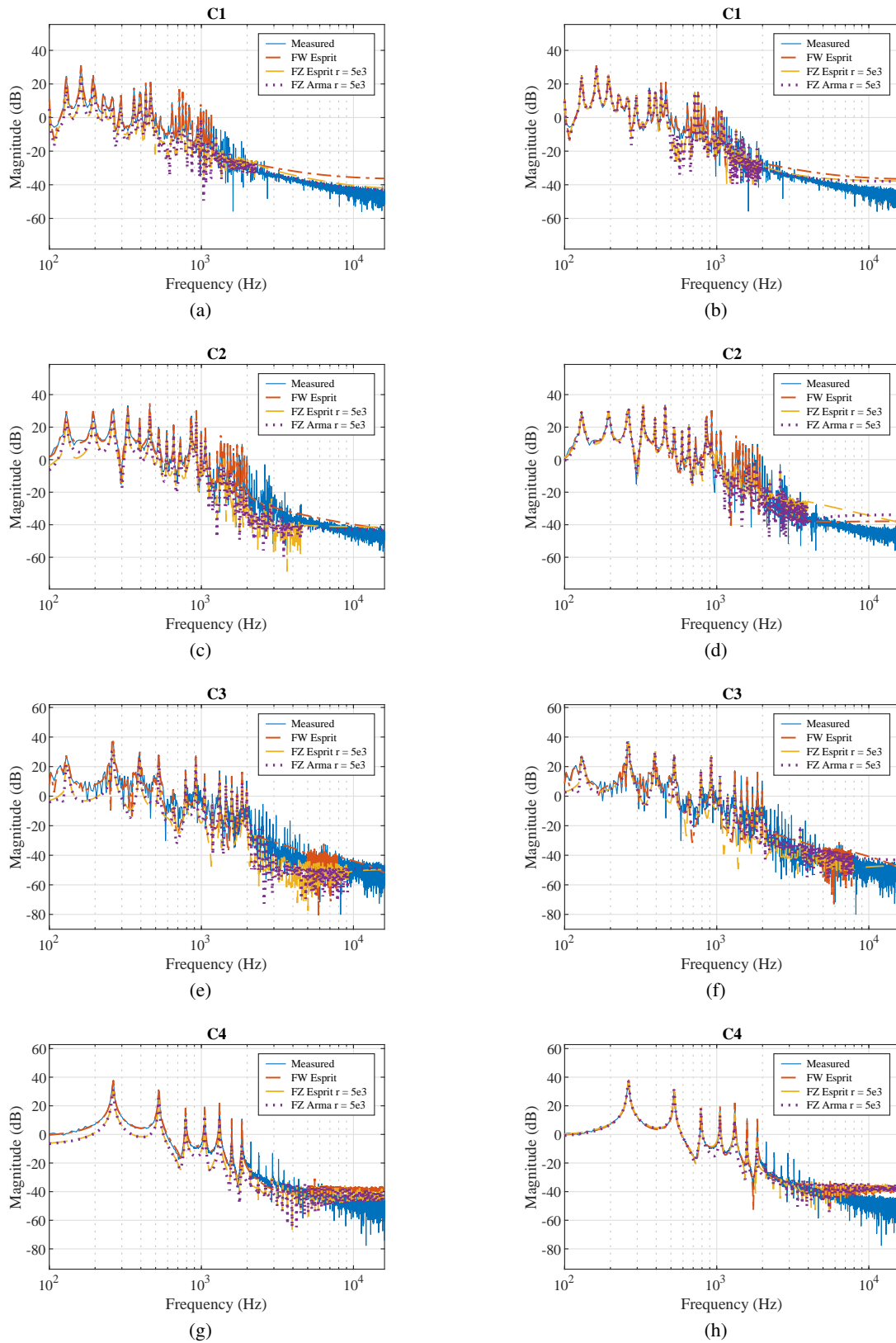


Figure 3: Frequency response of measured and synthesized notes. Left - without mode optimization, Right - with mode optimization.

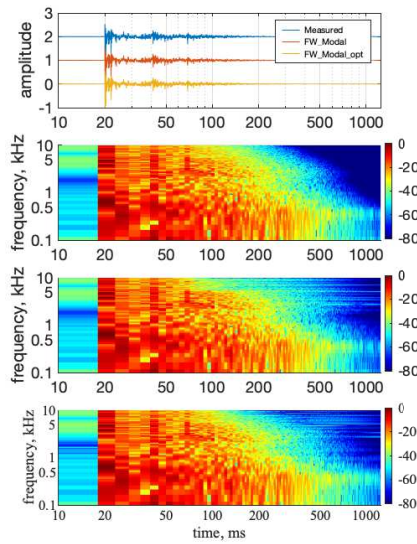
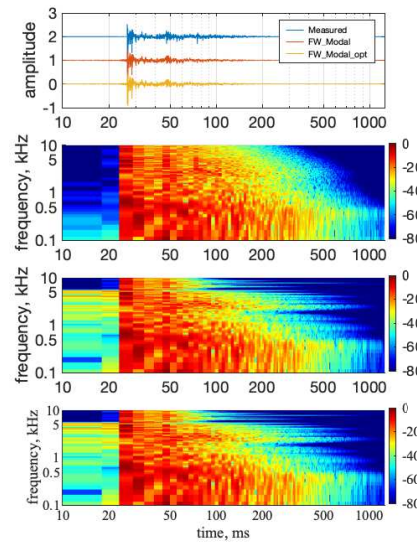
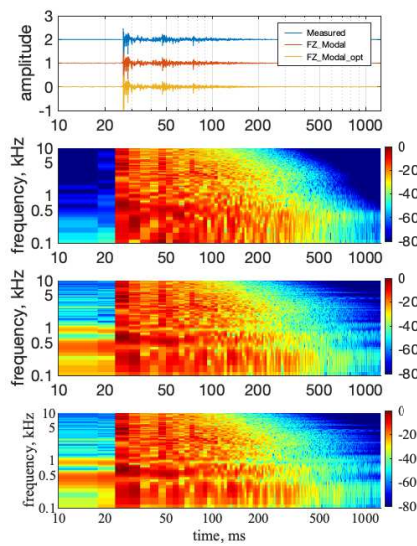
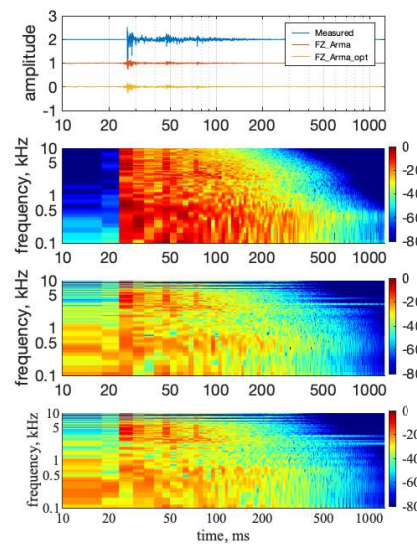
(a) FW-ESPRIT, $M = 2994$ (b) FW-ESPRIT, $M = 1402$ (c) FZ-ESPRIT, $M = 1421$ (d) FZ-ARMA, $M = 1368$

Figure 4: RIR modeling results. Spectrograms from top - Measured, Modeled without optimization, Modeled with optimization.